TISSUE ENGINEERING: Part C
Volume 19, Number 7, 2013
© Mary Ann Liebert, Inc.
DOI: 10.1089/ten.tec.2012.0495

Use of Micro-Computed Tomography to Nondestructively Characterize Biomineral Coatings on Solid Freeform Fabricated Poly (L-Lactic Acid) and Poly (ε-Caprolactone) Scaffolds *In Vitro* and *In Vivo*

Eiji Saito, PhD,[1] Darilis Suarez-Gonzalez, PhD,[2] Rameshwar R. Rao, MSE,[1] Jan P. Stegemann, PhD,[1] William L. Murphy, PhD,[2–4] and Scott J. Hollister, PhD[1,5,6]

Biomineral coatings have been extensively used to enhance the osteoconductivity of polymeric scaffolds. Numerous porous scaffolds have previously been coated with a bone-like apatite mineral through incubation in simulated body fluid (SBF). However, characterization of the mineral layer formed on scaffolds, including the amount of mineral within the scaffolds, often requires destructive methods. We have developed a method using micro-computed tomography (μ-CT) scanning to nondestructively quantify the amount of mineral *in vitro* and *in vivo* on biodegradable scaffolds made of poly (L-lactic acid) (PLLA) and poly (ε-caprolactone) (PCL). PLLA and PCL scaffolds were fabricated using an indirect solid freeform fabrication (SFF) technique to achieve orthogonally interconnected pore architectures. Biomineral coatings were formed on the fabricated PLLA and PCL scaffolds after incubation in modified SBF (mSBF). Scanning electron microscopy and X-ray diffraction confirmed the formation of an apatite-like mineral. The scaffolds were implanted into mouse ectopic sites for 3 and 10 weeks. The presence of a biomineral coating within the porous scaffolds was confirmed through plastic embedding and μ-CT techniques. Tissue mineral content (TMC) and volume of mineral on the scaffold surfaces detected by μ-CT had a strong correlation with the amount of calcium measured by the orthocresolphthalein complex-one (OCPC) method before and after implantation. There was a strong correlation between OCPC pre- and postimplantation and μ-CT measured TMC ($R^2 = 0.96$ preimplant; $R^2 = 0.90$ postimplant) and mineral volume ($R^2 = 0.96$ preimplant; $R^2 = 0.89$ postimplant). The μ-CT technique showed increases in mineral following implantation, suggesting that μ-CT can be used to nondestructively determine the amount of calcium on coated scaffolds.

Introduction

Porous scaffolds have been engineered using a variety of biodegradable materials, including poly (L-lactic acid) (PLLA), poly (lactide-co-glycolide acid) (PLGA), and poly (ε-caprolactone) (PCL) to repair bone defects. These materials are readily formed into three-dimensional (3D) architectures, degrade in desirable periods relative to bone formation, and are relatively radio transparent, which allows bone healing to be readily tracked by X-ray or computed tomography (CT). However, a significant disadvantage is their poor osteoconductivity compared to hydroxyapatite (HAP) and tricalcium phosphate scaffolds. Polymer scaffold osteoconductivity can be improved by deposition of a surface biomineral coating using a simulated body fluid (SBF) containing similar ion components to human blood plasma.[1–3]

Biomineralization has been successfully applied to various biomaterials, including polymers,[4–9] and the composites of polymers and HAP or other calcium phosphates.[6,10,11] The resulting coatings have been characterized *in vitro* using destructive methods, such as electron microscopy. However, the 3D distribution of mineral coatings within scaffold architectures has not been well characterized due to limitations in the destructive, inherently 2D techniques.

Micro-computed tomography (μ-CT) has been widely used to nondestructively assess fabricated architectures of biodegradable polymer and calcium phosphate scaffolds.[12–15] In this system, images are obtained by material

[1]Department of Biomedical Engineering, University of Michigan, Ann Arbor, Michigan.
[2]Materials Science Program, University of Wisconsin, Madison, Wisconsin.
Departments of [3]Biomedical Engineering and [4]Orthopedics and Rehabilitation, University of Wisconsin, Madison, Wisconsin.
Departments of [5]Mechanical Engineering and [6]Surgery, University of Michigan, Ann Arbor, Michigan.

attenuation of X-ray to evaluate scaffold geometry and simulate mechanical behavior.[13,14,16] The existence of biomineral coatings on polymer scaffold surfaces also have been examined using μ-CT since polymer is almost radio transparent compared to other radio-dense materials.[17–19] However, the 3D volume and distribution of mineral coating within porous scaffolds has not been precisely quantified and verified versus destructive methods. Furthermore, changes in mineral coating following implantation *in vivo* have not been rigorously quantified in 3D. The ability to rigorously quantify the volume and spatial distribution of coatings within 3D architectures following SBF incubation and track coating changes over time *in vivo* are unmet needs.

PLLA and PCL scaffolds have been fabricated with controlled porous architectures using computer-aided design and indirect solid freeform fabrication (SFF).[20–22] The advantage of using controlled architectures as opposed to conventional methods like particle leaching[23–26] is that the same architecture can be reproduced in different materials (like PLLA and PCL), allowing a direct comparison of substrate effects on mineral coating without different architectures confounding the results. Furthermore, the fully connected designed pore architectures enhance the ability to coat the architectures using fluid-based methods like SBF incubation.

We hypothesized that PLLA and PCL scaffolds with rigorously controlled pore architectures could be successfully coated with biomineral layers and that the biomineral coatings on the scaffolds could be nondestructively analyzed using μ-CT after *in vitro* and *in vivo* experiments. PLLA and PCL scaffolds were fabricated using an indirect SFF technique and subsequently coated with biomineral layers through incubation in a modified SBF (mSBF). The scaffolds were subcutaneously implanted in back of mice for 3 and 10 weeks. The morphologies and cross sections of the mineral coating were characterized using a scanning electron microscope (SEM), X-ray diffraction (XRD), and plastic embedding techniques to qualify the mineral coatings. The amount of mineral was quantified using a combination of μ-CT and calcium (Ca) measurements techniques before and after implantation.

Methods

Porous scaffold design and fabrication

Cylindrical porous PLLA and PCL scaffolds 5 mm diameter and 3 mm height were fabricated using an indirect SFF (Fig. 1).[21,27] Scaffolds were designed using image-based technique, where a unit cell with orthogonally interconnected pore channels was designed and then repeated in three dimensions to fill a desired scaffold outer dimension (5 × 3 mm).[28] Resulting image representations were converted to stereolithography (STL) formats and sliced in Modelworks software (Solidscape, Inc.) to fabricate wax molds using a PatternMaster™ 3D printer (Solidscape, Inc.). These wax molds were cast into HAP ceramic negative molds. Polymer pellets, PLLA (inherent viscosity = 0.65 dL/g; Birmingham Polymers Inc.) and PCL (molecular weight: 43,000–50,000; Polyscience Inc.), were heated at 205°C and 120°C, respectively, in a Teflon mold. The HAP molds were then placed into the Teflon mold containing molten polymer, in order to force the polymer through the open pore network.

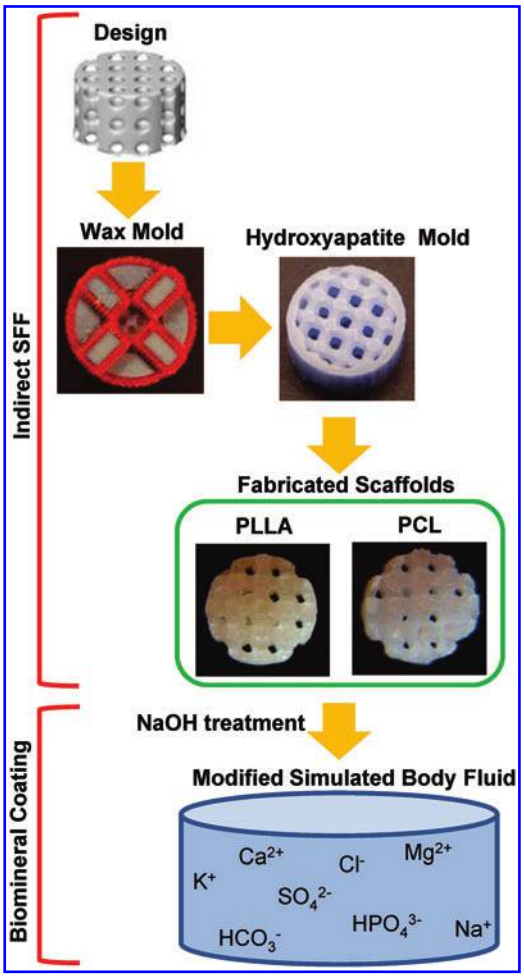

FIG. 1. Poly (L-lactic acid) (PLLA) and poly (ε-caprolactone) (PCL) with designed architectures were fabricated using indirect solid freeform fabrication. Fabricated scaffolds were simultaneously coated using modified simulated body fluid. Color images available online at www.liebertpub.com/tec

The HAP molds were removed from the porous polymer scaffolds using RDO Rapid Decalcifier (APEX Engineering Products Corp.) and washed with 100% ethanol.

Mineral coating incubation in mSBF

Fabricated PLLA and PCL scaffolds were coated in the same manner (Fig. 1). The scaffolds were hydrolyzed in a 0.1 M NaOH for 60 min to expose surface carboxylate anions and alcohol groups that serve as mineral nucleation sites. Subsequently, samples were rinsed at least three times with deionized H_2O. Scaffolds were incubated at 37°C in 15 mL of mSBF for 14 days under continuous rotation. The mSBF solution is similar to human plasma but with double the concentration of calcium and phosphate, and was prepared as previously reported.[17] Specifically, the following reagents were added to ddH_2O heated to 37°C in the order shown; 141 mM NaCl, 4.0 mM KCl, 0.5 mM $MgSO_4$, 1.0 mM $MgCl_2$, 4.2 mM $NaHCO_3$, 20.0 mM Tris, 5.0 mM $CaCl_2$, and 2.0 mM KH_2PO_4. The solution was then adjusted to a final pH of 6.8. The mSBF solution was renewed daily to maintain a consistent ionic strength and pH throughout the experiment.

Scaffold surface characterization by SEM

The surfaces of preimplanted scaffolds were examined in an environmental scanning electron microscope (ESEM), Philips XL30 ESEM. Imaging was performed in variable pressure mode at a pressure of 0.7Torr and at an accelerating voltage of 10 kV. Scaffold surfaces were further investigated using SEM with X-ray energy disperse spectroscopy (XEDS).

Preimplanted mineral-coated scaffolds were embedded in epoxy resin (Embed 812, Electron Microscopy Sciences), and postimplanted mineral coated scaffolds were embedded in methyl methacrylate (MMA) (Fisher Scientific), N-butyl methacrylate (Sigma-Aldrich), methyl benzoate (Sigma-Aldrich), and polyethylene glycol 400 (Fisher Scientific) as previously described.[29–31] The embedded specimens were sectioned with a microtome using a diamond blade (Isomet; Buehler) with 200–300 μm thickness. The cross sections were observed in backscattered electron imaging mode in an FEI Quanta focused ion beam workstation and environmental SEM, at a pressure of 0.5 Torr and at an accelerating voltage of 30 kV.

Mineral coating characterization by XRD

For XRD analysis, the mineral-coated scaffolds were immersed in chloroform (ACROS Organics) and stirred continuously for 20 min or until completely dissolved. The mixture was then centrifuged at 4000 rpm for 5 min to separate out the mineral component. The mineral was rinsed in fresh chloroform and centrifuged for a second time. After collecting the chloroform, the mineral powder was dried under the hood for 2 days to allow residual chloroform to evaporate for XRD analysis. XRD patterns were recorded using a General Area Detector Diffraction System, with a Hi-star 2-D area detector ($20° < 2\theta < 40°$) using Cu Kα radiation. The resulting patterns of the samples were identified by computer matching with an International Centre for Diffraction Data (ICDD) powder diffraction database (ICDD card number for HAP: 00-001-1008). XRD patterns of the coated scaffold surfaces were also measured in a nondestructive manner using a Bruker D8 Discover X-ray Diffractometer.

Cell preparation, virus infection and scaffold implantation in mice subcutaneous sites

Coated scaffolds were loaded with virally transduced human fibroblasts, as described in previous studies.[21,22] Primary human gingival fibroblasts (HGFs) (ScienCell) were cultured and expanded on passage 6 near confluence in Dulbecco's modification of Eagles medium (DMEM) supplemented with 10% fetal bovine serum, and 1% penicillin and streptomycin (Gibco). The HGFs were infected with AdCMV-GFP, a recombinant adenovirus construct expressing murine green fluorescent protein gene under a cytomegalovirus (CMV) promoter, at a multiplicity of infection of 500 PFU/cell for 20 h. About 0.5 million cells were seeded into each scaffold by suspending them in 40 μL of 5 mg/mL collagen gel. The gelation procedure was as follows: Rat-tail collagen high concentration (stock concentration = 9.03 mg/mL; BD Bioscience Discovery Labs) was diluted with cold sterile 0.02 N acetic acid to make 5 mg/mL. 0.5 N sodium hydroxide with 220 mg/mL sodium bicarbonate was added to Col I gel mixture to initiate gelation, and gel contents were mixed with cells and evenly re-suspended. Forty microliters of cell and gel mixture was placed in each hole of sterilized custom-made Teflon mold, and the scaffolds were placed on top of the gel to enforce infiltration. This was followed by incubation at 37°C for 40 min to solidify gels further. The scaffolds seeded with HGFs were transferred in ultra-low cluster 24-well plate (Corning Incorporated) with DMEM containing 2% FBS were incubated on an orbital shaker for 24 h.

The scaffolds were subcutaneously implanted into 6–7-week-old (46–53-day-old) female immunocompromised mice (NIHS-bg-nu-xid, Harlan). Animals were anesthetized with an injection of ketamine/xylazine, 4 subcutaneous pockets were created, and 4 scaffolds (one scaffold from each group) were implanted into each mouse. Surgical sites were closed with wound clips in compliance with the University of Michigan University Committee on Use and Care of Animal regulations. The mice were sacrificed at 3 and 10 weeks after the implantation, and the scaffold and tissue constructs were harvested, fixed with Z-fix (Anatech), and stored in 70% ethanol for further assay.

μ-CT analysis of fabricated scaffold architectures and amount of coated mineral

All of the scaffolds were scanned using an MS-130 high-resolution μ-CT Scanner (GE Medical Systems) at a resolution of 16 μm before and after implantation. The resulting data was analyzed using MicroView software (GE Healthcare). Mineral-coated scaffolds were scanned in Milli-Q water to enhance the contrast of the biomineral layer, and uncoated scaffolds were scanned in air due to polymer radio transparency when scanned in water. Total immersion time of the coated scaffolds in Milli-Q was kept to approximately 1.5 h (including scanning time) to minimize the potential error of mineral dissolution in the water. Each scan was calibrated with a calibration phantom containing air, water, and a material that mimics cortical bone. The calibration values of air and water were set to −1000 and 0 Hounsfield Units (HU), respectively, and the bone HU value was calculated using a standard conversion equation from air and water values.[32] The scanned scaffold images were reconstructed, stored as .vff files and then processed to determine the architecture of the uncoated scaffolds and the amount of mineral on the coated scaffolds.

Pore size, strut size, volume, and surface area were assessed to characterize uncoated scaffold architectures. Pore size was measured on three orthogonal planes and averaged to obtain the mean value for each scaffold. Strut sizes were measured as the material distance between the pores, and also averaged in the same manner as the pore size. The volume and surface area of each scaffold were calculated after applying an isodensity threshold using an Autothreshold function in MicroView to render 3D images, which generated threshold values of -542.5 ± 16.5 HU and -647.7 ± 20.3 HU for uncoated PLLA and uncoated PCL scaffolds, respectively.

To determine the amount of mineral on the scaffold surfaces, a cylindrical region of interest (ROI) with 5.6 mm diameter and 3.5 mm height was chosen to encompass the whole scaffold, and then the amount of mineral was

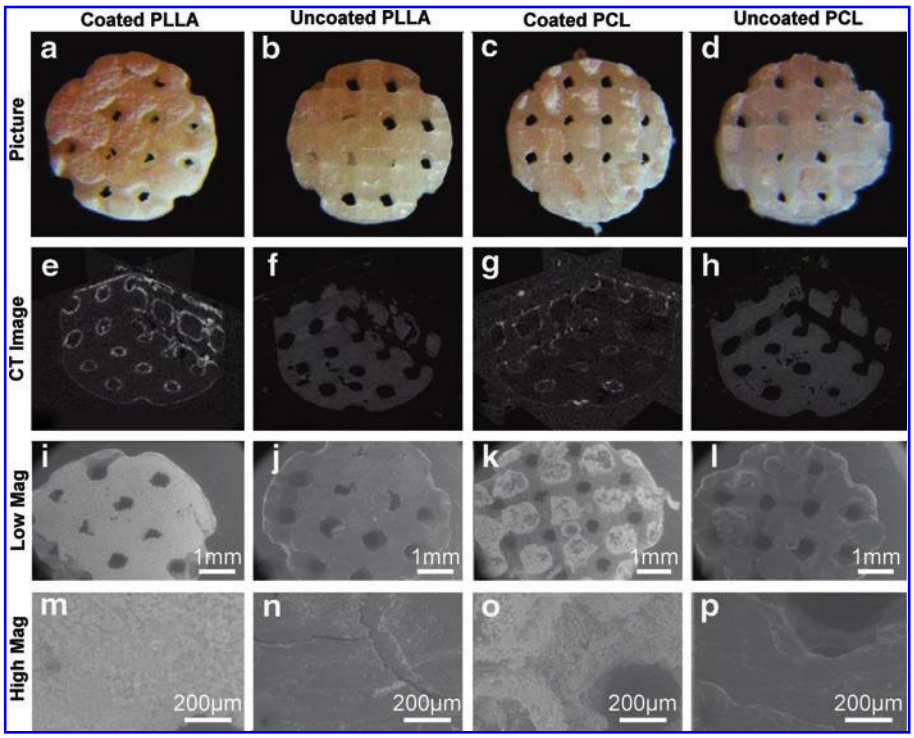

FIG. 2. Images, micro-computed tomography (μ-CT) images, and environmental scanning electron microscope (ESEM) images of coated PLLA **(a, e, i, m)**, uncoated PLLA **(b, f, j, n)**, coated PCL **(c, g, k, o)** and uncoated PCL **(d, h, l, p)**. μ-CT images confirm that mineral layer covered the surface of both PLLA and PCL scaffolds **(e, g)**. ESEM images show that rough surface of the coated PLLA and PCL scaffolds **(m, o)**, while relatively smooth surface of the uncoated PLLA and PCL scaffolds **(n, p)**. Color images available online at www.liebertpub.com/tec

calculated applying various threshold values from 400 to 800 HU by 50 HU increments, similar to techniques for detecting bone tissue.[33,34] The mineral content on the scaffolds after coating were calculated by subtracting the mineral content values before implantation from those after implantation within the ROI.

Calcium content of coated scaffolds

Scaffolds were dissolved in 1 mL of 1.0 N acetic acid for 3 days (preimplanted scaffolds) or 10 days (postimplanted scaffolds) to ensure all mineral was dissolved. Calcium deposited on scaffolds was quantified using an orthocresolphthalein complex-one (OCPC) method in which 10 μL of the dissolved solution was reacted with 300 μL of a working solution consisting of 0.05 mg/mL of OCPC solution and ethanolamine/boricacid/8-hydroxyquinoline buffer (Sigma) for 10 min at room temperature.[35] Samples were read spectrophotometrically at 575 nm, and calcium values were quantified by comparison to a standard curve prepared over a range of 0–100 μg/mL. Samples were diluted 50-fold as necessary. In addition, the scaffolds were re-immersed in acetic acid for three more days, and OCPC method was performed to confirm there was no remaining calcium on the scaffolds.

Statistical analysis

Statistical analysis was performed with SPSS (SPSS, Inc.). Two groups were analyzed with Student's *t*-test for independent samples. Multiple comparisons were evaluated by one-way ANOVA followed by Tukey's Post Hoc multiple comparisons. Errors are reported in figures as standard deviation (SD) and significance was determined using a probability value of $p < 0.05$.

Results

Morphology of coated and uncoated scaffolds

PLLA and PCL scaffolds had similar morphology, and become less transparent after mineral coating (Fig. 2a–d). Uncoated PLLA and PCL scaffold architectures were analyzed using μ-CT (Fig. 2f, h). Pore size, strut size, volume, surface area, and surface-to-volume ratio of uncoated PLLA and PCL scaffolds were measured ($N = 6$–7) (Table 1). These values were the same between the PLLA and PCL scaffolds, which indicates that the scaffolds had identical architectures. μ-CT data also showed the existence of 3D mineral layers inside of the scaffold architectures (Fig. 2e, g). Since the polymer has similar density to water, PLLA and PCL scaffolds were almost radio transparent and only mineral

Table 1. Micro-Computed Tomography Measurements of Fabricated Uncoated Poly (L-Lactic Acid) and Poly (ε-Caprolactone) Scaffolds

	Pore size (mm)	*Strut size (mm)*	*Volume (mm^3)*	*Surface (mm^2)*	*Surface/volume*
PLLA Scaffold	0.60 ± 0.03	0.67 ± 0.03	33.26 ± 2.19	187.13 ± 13.75	5.63 ± 0.20
PCL Scaffold	0.61 ± 0.04	0.67 ± 0.03	30.97 ± 1.29	182.22 ± 10.82	5.88 ± 0.13

PLLA, poly (L-lactic acid); PCL, poly (ε-caprolactone).

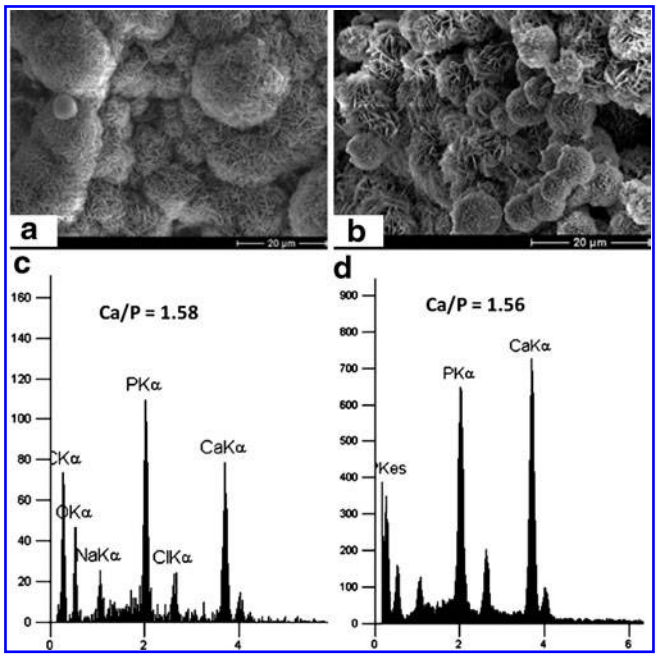

FIG. 3. Scanning electron microscopy (SEM) images and X-ray energy disperse spectroscopy (XEDS) data of coated minerals of PLLA **(a, c)** and PCL **(b, d)** scaffolds. SEM images show that nucleated bone like mineral structures on the coated PLLA and PCL scaffolds **(a, b)**. XEDS data confirmed that existence of calcium and phosphorous peaks **(c, d)**.

coatings were visible in the CT images. Scaffold surfaces were further characterized using ESEM (Fig. 2i–p). Uncoated PLLA and PCL scaffolds had smooth surfaces (Fig. 2j, l, n, p), while mineral coated PLLA and PCL scaffolds had rough surfaces (Fig. 2i, k, m, o).

Nanoscale plate-like crystalline structures were observed on both coated PLLA and PCL scaffolds (Fig. 3a, b) as observed in previous studies of mineral coatings on bioresorbable polymers. Analysis of biomineral composition by XEDS showed that the mineral was composed primarily of calcium and phosphorous with a Ca/P ratio of 1.58 for coated PLLA scaffold (Fig. 3c) and 1.56 for coated PCL scaffold (Fig. 3d), which are in the range of biological apatite. These data support growth of bone-like HAP minerals on the surface of the scaffolds.

Crystallinity

Both biomineral-coated PLLA and PCL scaffolds were dissolved in chloroform to obtain biomineral crystallinity (Fig. 4a,b). The data shows that coated PLLA and PCL scaffolds crystal peaks were similar to those of HAP. Crystallinity of the mineral-coated scaffolds was also detected without dissolving the polymer component in chloroform. The coated PLLA showed major peaks at $2\theta = 25.9$ and 31.95 (Fig. 4c), consistent with the major crystalline peaks of HAP, while the uncoated PLLA scaffold showed many peaks due to its semi-crystalline structures (Fig. 4d). In contrast, the coated PCL also clearly showed crystal peaks at $2\theta = 25.9$ and 31.95 (Fig. 4e), while the uncoated PCL scaffolds had amorphous structures and did not show crystal peaks of polymer (Fig. 4f).

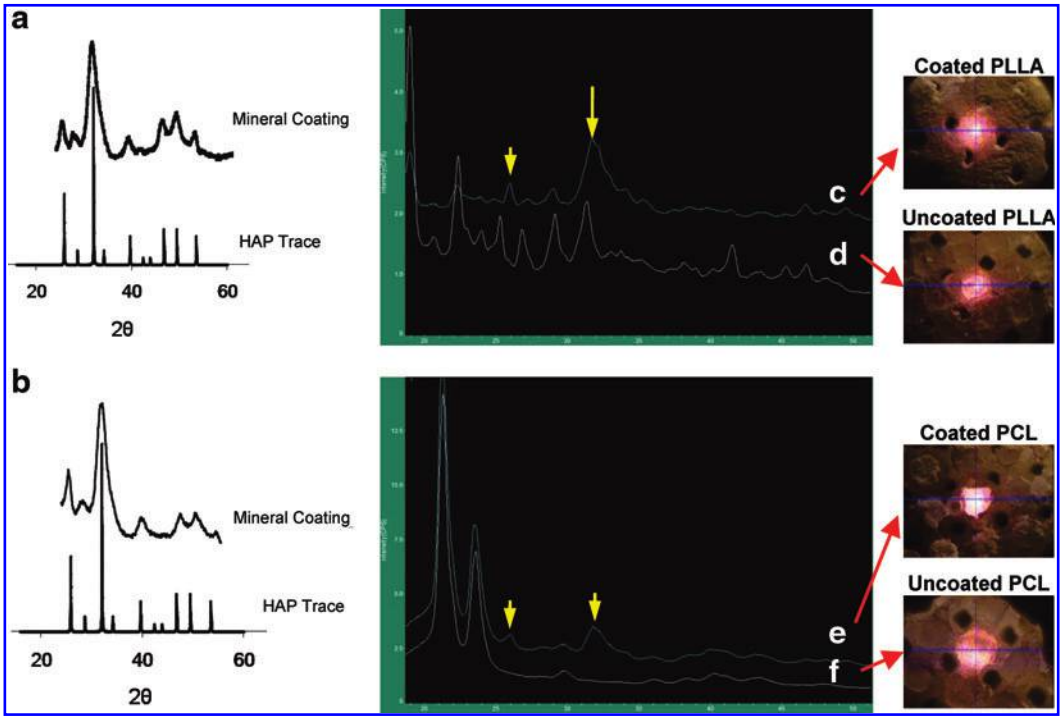

FIG. 4. X-ray diffraction (XRD) data was obtained mineral-coated scaffolds after dissolving them in chloroform, coated PLLA **(a)** and coated PCL **(b)**. Mineral peaks reflecting HAP pattern were shown. XRD data of surface of the scaffolds is also shown, coated PLLA **(c)**, uncoated PLLA **(d)**, coated PCL **(e)**, and uncoated PCL **(f)**, and the coated PLLA scaffold shows their peak at $2\theta = 25.9$ and 31.95 **(c)**, and the uncoated PLLA scaffold shows many peaks due to its semi-crystalline structures **(d)**. The coated PCL also show their crystal peaks at $2\theta = 25.9$ and 31.95 **(e)**. Color images available online at www.liebertpub.com/tec

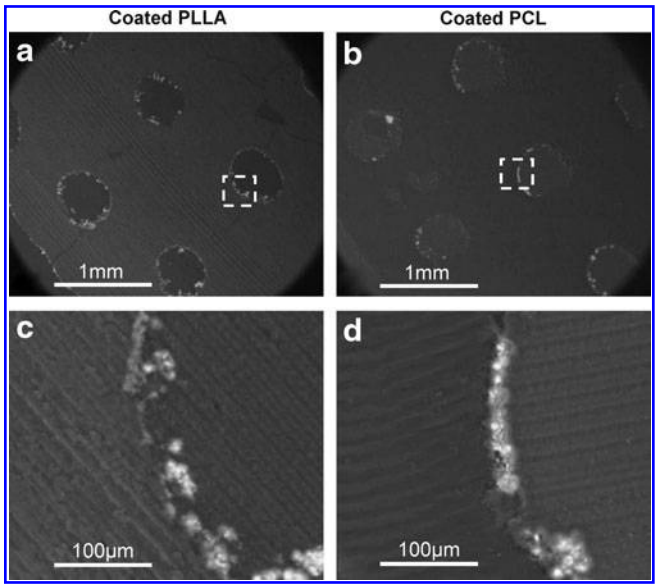

FIG. 5. SEM images of mineral-coated scaffolds embedded and sectioned in methyl methacrylate (MMA), coated PLLA **(a)** and coated PCL **(b)**. The magnified areas of yellow boxes are also shown, coated PLLA **(c)** and coated PCL **(d)**. Images show that mineral layers as white color and polymers, scaffold and MMA, as dark gray. The mineral layers existed on the surface of porous scaffolds within coated PLLA and PCL scaffolds.

Cross section of mineral-coated scaffolds

Figure 5 shows the SEM images of mineral-coated scaffolds, coated PLLA (a), and coated PCL (b). Images show mineral layers as white color and polymers, scaffold and MMA, as dark gray. The magnified areas of yellow boxes show the coating thickness ranging from 20 to 30 μm on the coated PLLA (Fig. 5c) and PCL scaffolds (Fig. 5d) with some discontinuous parts of mineral layers.

Determining the relation between μ-CT and calcium assay of preimplanted scaffolds

Various threshold values in CT images were applied to visualize the biomineral coating on PLLA and PCL scaffolds (Fig. 6a). Yellow indicates biomineral that has higher density than the applied threshold values, while white indicates biomineral with lower density than the threshold values. Changing the value, the images shows more background at lower threshold, and less biomineral coating was detected at higher threshold. To find the optimal relationship between tissue mineral content (TMC) from μ-CT and the amount of calcium, a range of threshold values were examined. For threshold values ranging from 400 to 800 HU by 50 HU, a value of 600 HU showed the highest R-squared value (0.96) (Fig. 6a, b). The relation between volume of mineral layers from μ-CT and amount of calcium also showed a strong correlation ($R^2 = 0.96$) (Fig. 6c). The results indicated that mineral density calculated by μ-CT is significantly correlated with the amount of calcium measured by OCPC method.

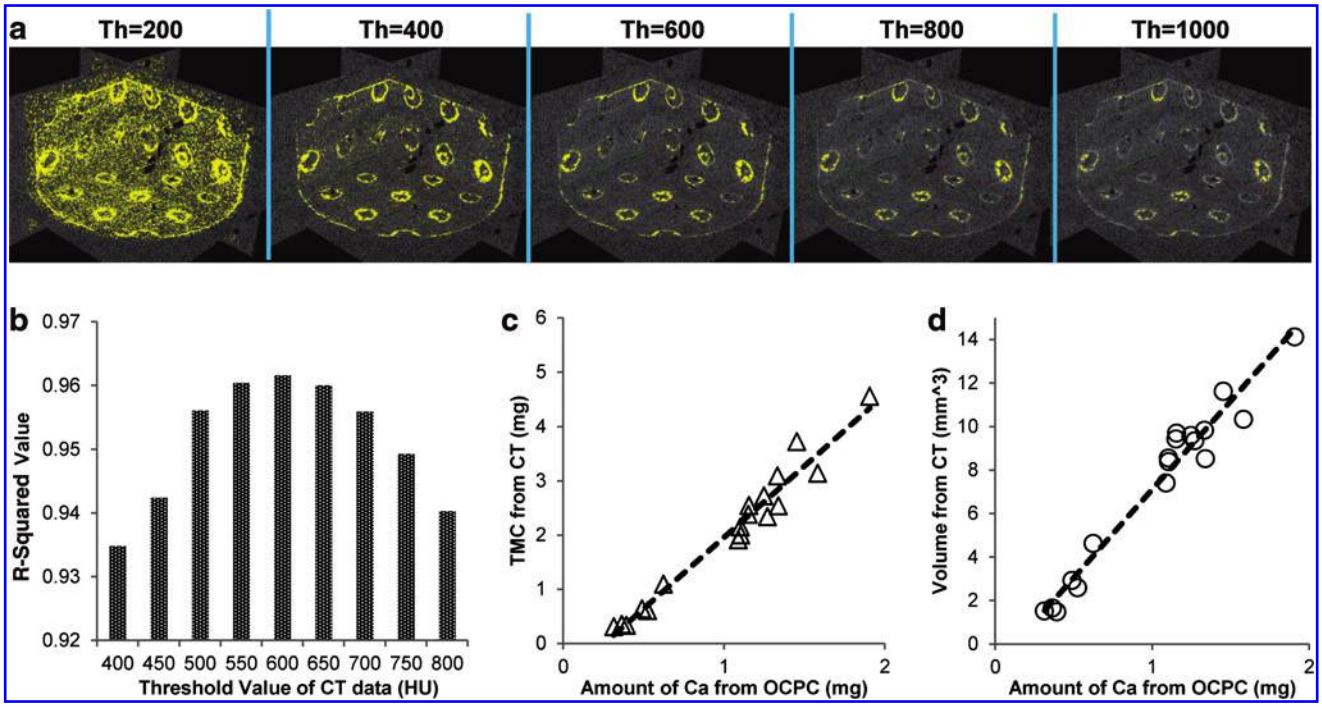

FIG. 6. Yellow color indicates biomineral coatings on the scaffold surface by varying the threshold values of μ-CT from 200 to 1000 **(a)**. R-squared values of correlation between amount of calcium (mg) from orthocresolphthalein complex-one (OCPC) method and tissue mineral content (mg) from μ-CT data **(b)**. Threshold values were varied from 400 to 800 HU by 50 HU, and the highest *R*-squared value (0.96) at threshold value with 600 HU. The relation between calcium amount and Tissue mineral content (TMC) **(c)** and volume from μ-CT data **(d)** are also shown. The *R*-squared values between calcium amount and volume from μ-CT data **(d)** is 0.96. Color images available online at www.liebertpub.com/tec

Uncoated PLLA and PCL scaffolds showed calcium values similar to background.

Mineral coatings on implanted scaffolds

Mineral coatings on the scaffolds after implantation were examined using backscattered SEM (Fig. 7). The images show that the mineral layers covered the scaffolds, following the scaffold architectures and pore outlines at 3 (Fig. 7a,c) and 10 (Fig. 7e, g) weeks implantation. From the magnified images, the thickness of the mineral layers observed at 3 weeks (Fig. 7b, d) at 10 weeks (Fig. 7f, h) indicates that the thickness does not decrease.

Quantifying biomineral coating on the scaffold after implantation

The implanted scaffolds were covered with soft tissue and the surface mineral was not visualized. The scaffolds with tissue were scanned in Milli-Q water using μ-CT. The data show that the mineral coating layers were observed throughout the study period on the coated scaffolds (Fig. 8a–d), and there is an apparent increase in the intensity of mineral coating at 10 weeks compared to 3 weeks. Although the scaffolds were covered with soft tissues, the tissues were close to radio transparent under μ-CT.

The amount of calcium on the implanted scaffolds surfaces was also measured using the OCPC method. The coated scaffolds showed the existence of calcium, while the uncoated scaffolds had calcium values similar to background. The relationship between TMC and the amount of calcium from OCPC were examined varying the threshold values from 400 to 800 HU. The highest R-squared value (0.90) was again obtained at a threshold value of 600 HU (Fig. 8e, f). The amount of calcium by OCPC again showed a strong correlation to mineral volume from μ-CT data with an *R*-squared value of 0.89 (Fig. 8g). Since mineral volume from μ-CT data are correlated with amount of calcium the OCPC assay, the amount of mineral before and after implantation were calculated from μ-CT data. The data shows that mineral volume increased after implantation (Fig. 9). The amount of deposited mineral layers calculated from μ-CT indicated significantly more mineral deposition at 10 weeks than 3 weeks for both the coated PLLA ($p=0.001$) and PCL ($p=0.029$) scaffolds ($N=6$). Furthermore, the 10-week implanted coated PLLA scaffolds had significantly more mineral deposition than the 3-week ($p=0.000$) and 10-week ($p=0.002$) implanted coated PCL scaffolds ($N=6$).

Discussion

Biomineral coatings have been applied to porous polymer scaffolds to improve bone regeneration. We demonstrated that a μ-CT technique can be used to quantify the amount of biomineral coatings on porous scaffolds before and after implantation. First, we demonstrated that our mSBF technique was applicable to two different biodegradable scaffolds made of PLLA and PCL using indirect SFF. The mineral morphology and composition on the scaffold surfaces were confirmed using conventional techniques, SEM and XRD. Mineral coatings within the porous scaffolds were shown using plastic embedding and μ-CT techniques. Finally, the amount of minerals in each scaffold was quantified using μ-CT and compared with OCPC techniques, which provided a standard for the μ-CT based quantification.

By fabricating scaffolds using indirect SFF, it was possible to achieve two important objectives. First, the same architecture could be built from two different biomaterials, allowing us to test coating effects on two different material substrates without the confounding effects of different architectures. Second, fully connected pore structures could be created by indirect SFF.[21,22] The fabricated PLLA and PCL scaffolds were characterized using μ-CT to confirm that both

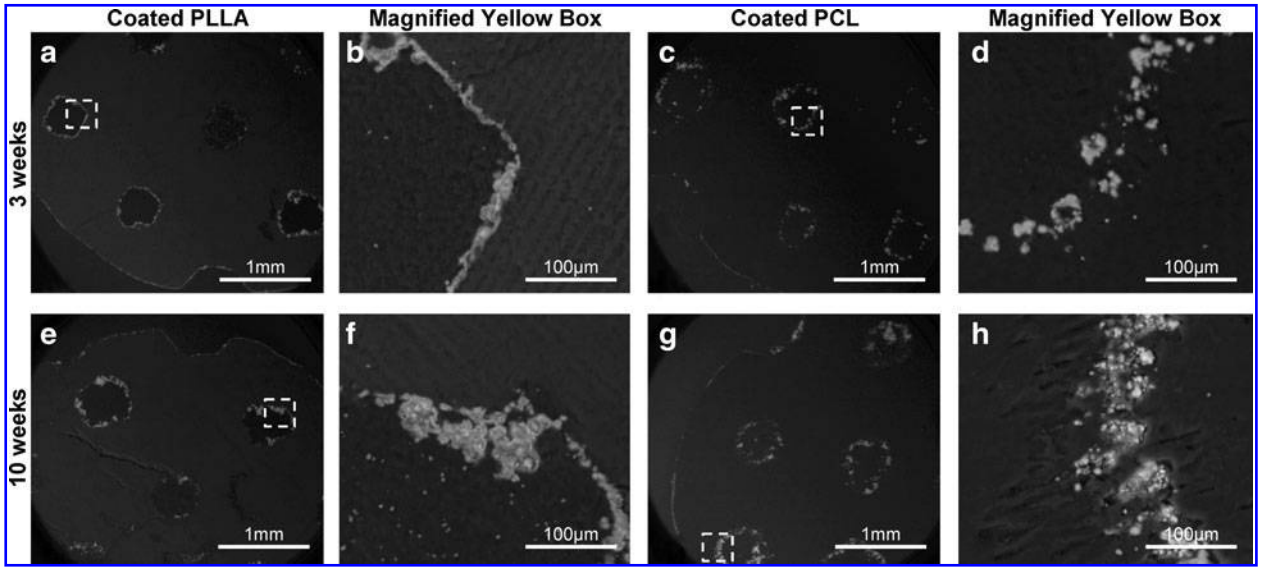

FIG. 7. Cross section of the implanted coated PLLA and PCL scaffolds at 3 **(a, c)** and 10 **(e, g)** weeks postimplantation, respectively. The mineral layers existed on the scaffold surfaces, following the scaffold architectures and pore outlines. The magnified areas of the yellow boxes are also shown, coated PLLA and coated PCL, at 3 **(b, d)** and 10 **(f, h)** weeks, respectively. The thickness of the mineral layers observed indicates that the thickness does not decrease.

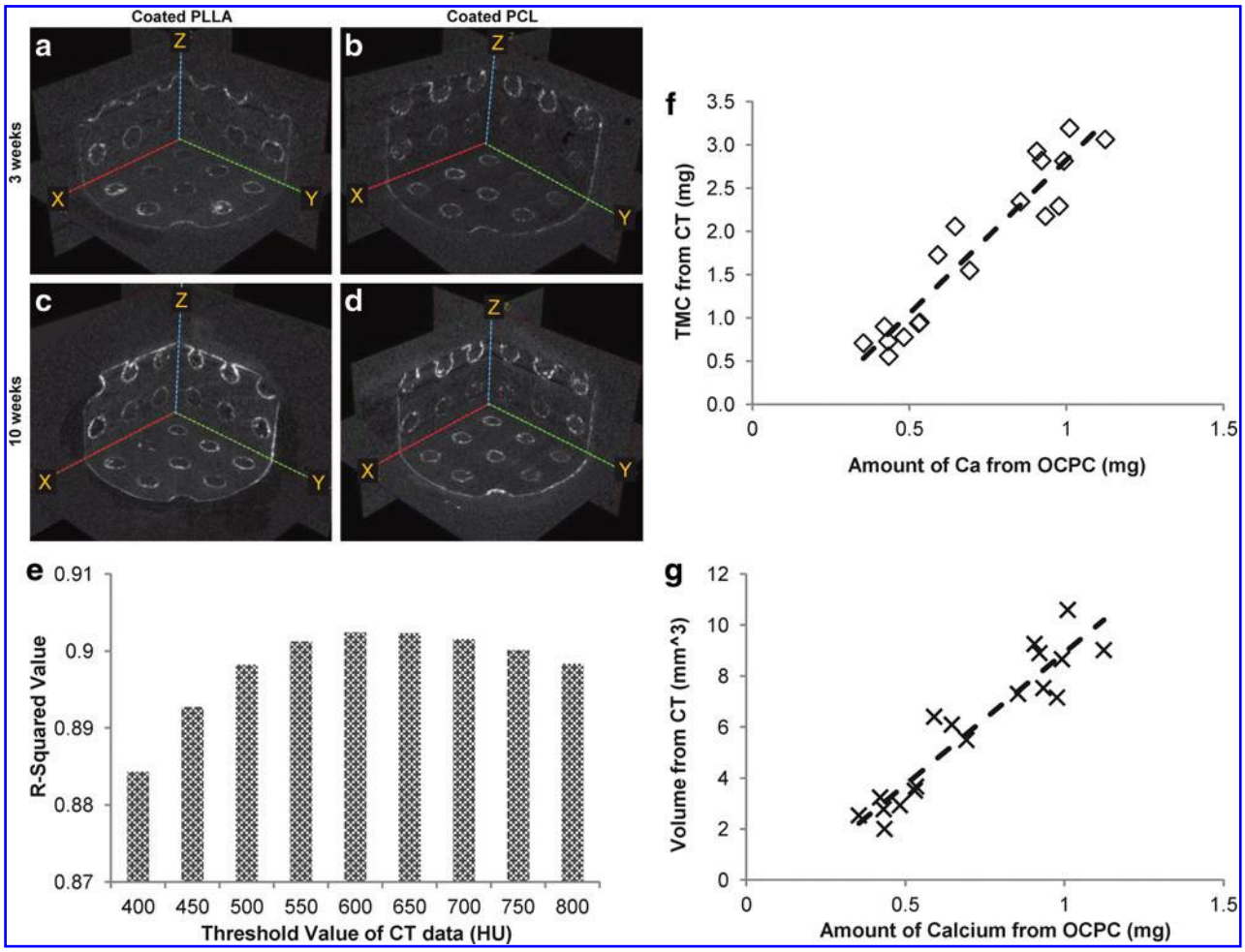

FIG. 8. μ-CT images of implanted coated PLLA at 3 **(a)** and 10 **(c)** weeks, and implanted coated PCL at 3 **(b)** and 10 **(d)** weeks. *R*-squared values of correlation between amount of calcium (mg) from OCPC method and tissue mineral content (mg) from μ-CT data **(e)**. Threshold values were varied from 400 to 800 HU by 50 HU, and the highest *R*-squared value (0.90) were achieved at threshold with 600 HU, as the relation shown **(f)**. The calcium amount and volume from μ-CT data were correlated strongly with *R*-squared value of 0.89 **(g)**. Color images available online at www.liebertpub.com/tec

scaffolds had identical fully interconnected pore architectures that would allow efficient penetration of SBF to the scaffold interior.

The fabricated PLLA and PCL scaffolds were treated with mSBF, and the successful growth of biomineral surface coatings was confirmed. SEM images of mineral morphologies show plate-like structures, calcium to phosphorous ratio and crystal peaks similar to our previous studies of mineral-coated hydrogels, bioceramics, and biodegradable polymers.[17,36–39] XRD results showed both coated scaffolds showed crystal peaks of mineral at 26° and 32°, which correspond to the (002) plane and (211) (112) planes of apatite.[40] Coated PLLA showed a peak at 32°, and other peaks due to the crystal structure of PLLA polymer, which were confirmed from the XRD data of uncoated PLLA scaffolds.[41] In contrast, coated PCL showed two peaks from the PCL polymer around 21° and 24°, similar to previous studies.[36,42] All of these data confirm that the PLLA and PCL scaffolds were successfully coated with biomineral layers similar to those of previous studies using destructive (OCPC, XRD, and SEM) and nondestructive (μ-CT) methods.

It is very important to assess mineral coatings within porous architectures, such as thickness of mineral layer, which has been done via cutting or breaking without embedding.[18] However, these techniques were not applicable to SFF scaffolds, especially PLLA and PLGA scaffolds, since they are much stiffer than scaffolds fabricated using porogen leaching methods.[16,21] Therefore, to access the cross section of the mineral layers, plastic embedding techniques were utilized and showed the mineral layers covered the inside of the porous scaffolds and also followed the SFF scaffolds architectures. This section technique allowed demonstration of coating on both pre- and postimplanted scaffolds by SEM without losing the scaffold structures.

μ-CT has been utilized to achieve nondestructive quantification of 3D mineral coatings on porous scaffolds. Since the density of the polymer is lower than that of mineral and close to water, the scaffolds scanned in water helped make the polymer invisible and increase intensity of mineral coating.[14] Although previous studies showed that μ-CT may be applicable to monitor *in vitro* mineralization of porous scaffolds,[19,43,44] the accuracy of measured mineral coatings

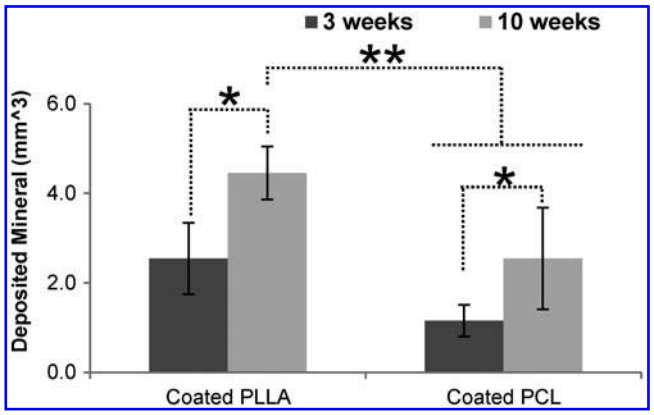

FIG. 9. The amount of deposited mineral layers calculated from μ-CT where the differences of mineral volume were calculated by subtracting postimplant scaffolds from preimplant scaffolds. There were significantly more mineral deposition at 10 weeks than 3 weeks for both the coated PLLA ($p=0.001$) and PCL ($p=0.029$) scaffolds *($N=6$). Furthermore, the 10-week implanted coated PLLA scaffolds had significantly more mineral deposition than the 3-week ($p=0.000$) and 10-week ($p=0.007$) implanted PCL scaffolds **($N=6$).

by μ-CT has not been examined. Therefore, to evaluate the accuracy of μ-CT data and qualify the amount of mineral, TMC and mineral volume from μ-CT data were compared with the amount of calcium in the mineral layers using OCPC method which has been used to characterize biomineral coatings.[35,45]

TMC from μ-CT and OCPC data showed a strong correlation when the threshold values ranged from 400 to 800 HU. However, *R*-squared values and image contrasts of mineral parts were varied by changing the threshold values of the μ-CT data, indicating the importance of choosing proper threshold values. The optimized threshold value, 600 HU, was found to produce a strong correlation between μ-CT and OCPC data of the preimplanted scaffolds. Then, comparison between μ-CT and OCPC data was further performed on the postimplanted scaffolds. The soft tissue covering the scaffolds was less visible due to the low x-ray contrast of nonmineralized tissues,[46] which allowed examination of the mineral layers of the scaffolds. The μ-CT data showed strong correlation with OCPC data at the same optimal threshold value of 600 HU with the preimplanted scaffolds although the *R*-squared value was not as strong that of the preimplanted scaffolds. This may be because soft tissue covering the scaffolds interrupts dissolution of calcium or intensity of minerals in μ-CT data. Our study further proves that μ-CT can be used to quantify relative changes to biomineral coatings on both pre- and post-implanted scaffolds and suggest proper necessity of threshold values for mineral quantification.

Based on a strong correlation between the μ-CT data and calcium assay, we further applied μ-CT analysis to calculate mineral the difference in the amount of before and after implantation. The data showed a slight but significant increase of mineral on the scaffolds with longer implantation, while the SEM images only showed the 2D existence of mineral on the scaffold surface. These results support the use of μ-CT as a nondestructive method to assess the change in mineralization on the same scaffold before and after implantation. In future work, an *in vivo* μ-CT system may be used to track the change of minerals on scaffold surfaces without harvesting scaffolds.

The μ-CT data of the scaffolds with GFP-transduced HGFs demonstrated an increasing mineral layer accumulation on the scaffold, similar to that previously seen with carbonate apatite absorption in rat ectopic sites.[47] Although we have not investigated the mechanism of biomineral deposition *in vivo*, the observed slight increase in mineral content between week 3 and week 10 of implantation could potentially be due to a heterogeneous precipitation of new mineral on the initial mineral coatings, as the *in vivo* environment is often supersaturated with respect to HAP mineral. It is less likely that mineralized tissue is being formed within the scaffolds as ectopic mineralized tissue formation has not been commonly observed in rodent subcutaneous sites. Further study is needed into the mechanism for the observed increase in mineral content over time *in vivo*.

A limitation of this study is that the method used to quantify minerals using μ-CT may not be applicable in its current form when mineral-coated scaffolds are implanted long term into bony sites due to the difficulty of separating initial biomineral coating and newly growing bone tissue. It also needs to be noted that the optimal thresholds may vary depending on biomineral coating techniques with different mineral morphologies, necessitation further study of the relation between optimal threshold values and various biomineral techniques.

Conclusions

Biomineral coating has been applied to porous scaffolds to improve bone regeneration. We have applied biomineral coating on SFF PLLA and PCL scaffolds to ensure that mineral coatings were achieved within the same porous architecture. Biomineral layers were confirmed to have similar quantity to previously reported mineral coatings on 3D porous architectures. Furthermore, μ-CT was utilized to qualify and quantify the amount biomineral coating within the scaffolds in a nondestructive manner. The nondestructive μ-CT results showed a strong correlation with destructive OCPC calcium characterization, validating the use of μ-CT to verify the effect of ectopic implantation on coating evolution.

Acknowledgments

This study was supported by the National Institute of Health (NIH) R01 grant AR 053379 and R21 grant DE 022439. Dr. Darilis Suarez-Gonzalez is supported by NIH T32 DC009401. The authors also would like to thank for Prof. William Giannobile and Prof. Junro Yamashita in School of Dentistry, and Dr. Claire Jeong in Department of Biomedical Engineering at the University of Michigan for their supply of embedding reagents, use of the microtome and technical supports, and Prof. Paul Krebsbach in School of Dentistry at the University of Michigan for supply for GFP virus. We would like to acknowledge Prof. Steve Goldstein's lab at the University of Michigan for their kindness of use of the μ-CT systems.

Disclosure Statement

Prof. Scott J. Hollister and Prof. William L. Murphy are cofounders and shareholders in Tissue Regeneration Systems, Inc.

References

1. Chou, Y.F., Huang, W., Dunn, J.C., Miller, T.A., and Wu, B.M. The effect of biomimetic apatite structure on osteoblast viability, proliferation, and gene expression. Biomaterials **26,** 285, 2005.
2. Kretlow, J.D., and Mikos, A.G. Review: mineralization of synthetic polymer scaffolds for bone tissue engineering. Tissue Eng **13,** 927, 2007.
3. Liu, Y., Wu, G., and de Groot, K. Biomimetic coatings for bone tissue engineering of critical-sized defects. J R Society, Interface **7 Suppl 5,** S631, 2010.
4. Murphy, W.L., Kohn, D.H., and Mooney, D.J. Growth of continuous bonelike mineral within porous poly(lactide-co-glycolide) scaffolds *in vitro*. J Biomed Mater Res **50,** 50, 2000.
5. Murphy, W.L., and Mooney, D.J. Bioinspired growth of crystalline carbonate apatite on biodegradable polymer substrata. J Am Chem Soc **124,** 1910, 2002.
6. Chim, H., Hutmacher, D.W., Chou, A.M., Oliveira, A.L., Reis, R.L., Lim, T.C., and Schantz, J.T. A comparative analysis of scaffold material modifications for load-bearing applications in bone tissue engineering. Int J Oral Maxillofac Surg **35,** 928, 2006.
7. Holmbom, J., Sodergard, A., Ekholm, E., Martson, M., Kuusilehto, A., Saukko, P., and Penttinen, R. Long-term evaluation of porous poly(epsilon-caprolactone-co-L-lactide) as a bone-filling material. J Biomed Mater Res Part A **75,** 308, 2005.
8. Gorna, K., and Gogolewski, S. Preparation, degradation, and calcification of biodegradable polyurethane foams for bone graft substitutes. J Biomed Mater Res Part A **67,** 813, 2003.
9. Davis, H.E., Rao, R.R., He, J., and Leach, J.K. Biomimetic scaffolds fabricated from apatite-coated polymer microspheres. J Biomed Mater Res Part A **90,** 1021, 2009.
10. Kim, S.S., Park, M.S., Gwak, S.J., Choi, C.Y., and Kim, B.S. Accelerated bonelike apatite growth on porous polymer/ceramic composite scaffolds *in vitro*. Tissue Eng **12,** 2997, 2006.
11. Lickorish, D., Guan, L., and Davies, J.E. A three-phase, fully resorbable, polyester/calcium phosphate scaffold for bone tissue engineering: evolution of scaffold design. Biomaterials **28,** 1495, 2007.
12. Lin, A.S., Barrows, T.H., Cartmell, S.H., and Guldberg, R.E. Microarchitectural and mechanical characterization of oriented porous polymer scaffolds. Biomaterials **24,** 481, 2003.
13. Ho, S.T., and Hutmacher, D.W. A comparison of micro CT with other techniques used in the characterization of scaffolds. Biomaterials **27,** 1362, 2006.
14. van Lenthe, G.H., Hagenmuller, H., Bohner, M., Hollister, S.J., Meinel, L., and Muller, R. Nondestructive micro-computed tomography for biological imaging and quantification of scaffold-bone interaction *in vivo*. Biomaterials **28,** 2479, 2007.
15. Peyrin, F., Mastrogiacomo, M., Cancedda, R., and Martinetti, R. SEM and 3D synchrotron radiation micro-tomography in the study of bioceramic scaffolds for tissue-engineering applications. Biotechnol Bioeng **97,** 638, 2007.
16. Saito, E., Kang, H., Taboas, J.M., Diggs, A., Flanagan, C.L., and Hollister, S.J. Experimental and computational characterization of designed and fabricated 50:50 PLGA porous scaffolds for human trabecular bone applications. J Mater Sci Mater Med **21,** 2371, 2010.
17. Suarez-Gonzalez, D., Barnhart, K., Saito, E., Vanderby, R.,Jr, Hollister, S.J., and Murphy, W.L. Controlled nucleation of hydroxyapatite on alginate scaffolds for stem cell-based bone tissue engineering. J Biomed Mater Res Part A **95,** 222, 2010.
18. Oliveira, A.L., Malafaya, P.B., Costa, S.A., Sousa, R.A., and Reis, R.L. Micro-computed tomography (micro-CT) as a potential tool to assess the effect of dynamic coating routes on the formation of biomimetic apatite layers on 3D-plotted biodegradable polymeric scaffolds. J Mater Sci Mater Med **18,** 211, 2007.
19. Segvich, S., Smith, H.C., Luong, L.N., and Kohn, D.H. Uniform deposition of protein incorporated mineral layer on three-dimensional porous polymer scaffolds. J Biomed Mater Res Part B Appl Biomater **84,** 340, 2008.
20. Hollister, S.J. Porous scaffold design for tissue engineering. Nat Mater **4,** 518, 2005.
21. Saito, E., Liao, E.E., Hu, W.W., Krebsbach, P.H., and Hollister, S.J. Effects of designed PLLA and 50:50 PLGA scaffold architectures on bone formation *in vivo*. J Tissue Eng Regen Med 2011. [Epub ahead of print]; DOI: 10.1002/term.497.
22. Roosa, S.M., Kemppainen, J.M., Moffitt, E.N., Krebsbach, P.H., and Hollister, S.J. The pore size of polycaprolactone scaffolds has limited influence on bone regeneration in an *in vivo* model. J Biomed Mater Res Part A **92,** 359, 2010.
23. Melchels, F.P., Barradas, A.M., van Blitterswijk, C.A., de Boer, J., Feijen, J., and Grijpma, D.W. Effects of the architecture of tissue engineering scaffolds on cell seeding and culturing. Acta Biomater **6,** 4208, 2010.
24. Choi, S.W., Zhang, Y., and Xia, Y. Three-dimensional scaffolds for tissue engineering: the importance of uniformity in pore size and structure. Langmuir **26,** 19001, 2010.
25. Lee, K.W., Wang, S., Dadsetan, M., Yaszemski, M.J., and Lu, L. Enhanced cell ingrowth and proliferation through three-dimensional nanocomposite scaffolds with controlled pore structures. Biomacromolecules **11,** 682, 2010.
26. Kim, K., Dean, D., Wallace, J., Breithaupt, R., Mikos, A.G., and Fisher, J.P. The influence of stereolithographic scaffold architecture and composition on osteogenic signal expression with rat bone marrow stromal cells. Biomaterials **32,** 3750, 2011.
27. Saito, E., Liu, Y., Migneco, F., and Hollister, S.J. Strut size and surface area effects on long-term *in vivo* degradation in computer designed poly(l-lactic acid) three-dimensional porous scaffolds. Acta Biomater **8,** 2568, 2012.
28. Hollister, S.J., Levy, R.A., Chu, T.M., Halloran, J.W., and Feinberg, S.E. An image-based approach for designing and manufacturing craniofacial scaffolds. Int J Oral Maxillofac Surg **29,** 67, 2000.
29. Chang, P.C., Seol, Y.J., Cirelli, J.A., Pellegrini, G., Jin, Q., Franco, L.M., Goldstein, S.A., Chandler, L.A., Sosnowski, B., and Giannobile, W.V. PDGF-B gene therapy accelerates bone engineering and oral implant osseointegration. Gene Ther **17,** 95, 2010.
30. Erben, R.G. Embedding of bone samples in methylmethacrylate: an improved method suitable for bone histomorphometry, histochemistry, and immunohistochemistry. J Histochem Cytochem **45,** 307, 1997.
31. Nyman, J.S., Lynch, C.C., Perrien, D.S., Thiolloy, S., O'Quinn, E.C., Patil, C.A., Bi, X., Pharr, G.M., Mahadevan-Jansen, A., and Mundy, G.R. Differential effects between the loss of MMP-2 and MMP-9 on structural and tissue-level properties of bone. J Bone Miner Res **26,** 1252, 2011.
32. Meganck, J.A., Kozloff, K.M., Thornton, M.M., Broski, S.M., and Goldstein, S.A. Beam hardening artifacts in micro-computed tomography scanning can be reduced by X-ray

beam filtration and the resulting images can be used to accurately measure BMD. Bone **45,** 1104, 2009.
33. Pettway, G.J., Schneider, A., Koh, A.J., Widjaja, E., Morris, M.D., Meganck, J.A., Goldstein, S.A., and McCauley, L.K. Anabolic actions of PTH (1–34): use of a novel tissue engineering model to investigate temporal effects on bone. Bone **36,** 959, 2005.
34. Taylor, D.K., Meganck, J.A., Terkhorn, S., Rajani, R., Naik, A., O'Keefe, R.J., Goldstein, S.A., and Hankenson, K.D. Thrombospondin-2 influences the proportion of cartilage and bone during fracture healing. J Bone Miner Res **24,** 1043, 2009.
35. Rao, R.R., Jiao, A., Kohn, D.H., and Stegemann, J.P. Exogenous mineralization of cell-seeded and unseeded collagen-chitosan hydrogels using modified culture medium. Acta Biomater **8,** 1560, 2012.
36. Suarez-Gonzalez, D., Barnhart, K., Migneco, F., Flanagan, C., Hollister, S.J., and Murphy, W.L. Controllable mineral coatings on PCL scaffolds as carriers for growth factor release. Biomaterials **33,** 713, 2012.
37. Suarez-Gonzalez, D., Lee, J.S., Lan Levengood, S.K., Vanderby, R.,Jr, and Murphy, W.L. Mineral coatings modulate beta-TCP stability and enable growth factor binding and release. Acta Biomater **8,** 1117, 2012.
38. Lee, J.S., Suarez-Gonzalez, D., and Murphy, W.L. Mineral coatings for temporally controlled delivery of multiple proteins. Adv Mater (Deerfield Beach, Fla.) **23,** 4279, 2011.
39. Jongpaiboonkit, L., Franklin-Ford, T., and Murphy, W.L. Growth of hydroxyapatite coatings on biodegradable polymer microspheres. ACS Appl Mater Interfaces **1,** 1504, 2009.
40. Chen, Y., Mak, A.F., Li, J., Wang, M., and Shum, A.W. Formation of apatite on poly(alpha-hydroxy acid) in an accelerated biomimetic process. J Biomed Mater Res Part B Appl Biomater **73,** 68, 2005.
41. Yokoyama, Y., Oyane, A., and Ito, A. Biomimetic coating of an apatite layer on poly(L-lactic acid); improvement of adhesive strength of the coating. J Mater Sci Mater Med **18,** 1727, 2007.
42. Kim, H.W., Knowles, J.C., and Kim, H.E. Development of hydroxyapatite bone scaffold for controlled drug release via poly(epsilon-caprolactone) and hydroxyapatite hybrid coatings. J Biomed Mater Res Part B Appl Biomater **70**, 240, 2004.
43. Cartmell, S., Huynh, K., Lin, A., Nagaraja, S., and Guldberg, R. Quantitative microcomputed tomography analysis of mineralization within three-dimensional scaffolds *in vitro*. J Biomed Mater Res Part A **69,** 97, 2004.
44. Hagenmuller, H., Hofmann, S., Kohler, T., Merkle, H.P., Kaplan, D.L., Vunjak-Novakovic, G., Muller, R., and Meinel, L. Non-invasive time-lapsed monitoring and quantification of engineered bone-like tissue. Ann Biomed Eng **35,** 1657, 2007.
45. ter Brugge, P.J., Wolke, J.G., and Jansen, J.A. Effect of calcium phosphate coating crystallinity and implant surface roughness on differentiation of rat bone marrow cells. J Biomed Mater Res **60,** 70, 2002.
46. Metscher, B.D. MicroCT for comparative morphology: simple staining methods allow high-contrast 3D imaging of diverse non-mineralized animal tissues. BMC Physiol **9,** 11, 2009.
47. Barrere, F., van der Valk, C.M., Dalmeijer, R.A., van Blitterswijk, C.A., de Groot, K., and Layrolle, P. *In vitro* and *in vivo* degradation of biomimetic octacalcium phosphate and carbonate apatite coatings on titanium implants. J Biomed Mater Res Part A **64,** 378, 2003.

Address correspondence to:
Scott J. Hollister, PhD
Department of Biomedical Engineering
University of Michigan
Ann Arbor, MI 48109-2099

E-mail: scottho@umich.edu

Received: August 15, 2012
Accepted: November 1, 2012
Online Publication Date: March 8, 2013

This article has been cited by:

1. Hongwei Wu, Pengfei Lei, Gengyan Liu, Yu Shrike Zhang, Jingzhou Yang, Longbo Zhang, Jie Xie, Wanting Niu, Hua Liu, Jianming Ruan, Yihe Hu, Chaoyue Zhang. 2017. Reconstruction of Large-scale Defects with a Novel Hybrid Scaffold Made from Poly(L-lactic acid)/Nanohydroxyapatite/Alendronate-loaded Chitosan Microsphere: in vitro and in vivo Studies. *Scientific Reports* **7**:1. . [Crossref]
2. Shin Kyungsup, Acri Timothy, Geary Sean, Salem Aliasger K.. 2017. Biomimetic Mineralization of Biomaterials Using Simulated Body Fluids for Bone Tissue Engineering and Regenerative Medicine. *Tissue Engineering Part A* **23**:19-20, 1169-1180. [Abstract] [Full Text HTML] [Full Text PDF] [Full Text PDF with Links]
3. Dr. Kyungsup Shin, Dr. Timothy Acri, Dr. Sean Geary, Prof. Aliasger K Salem. Biomimetic Mineralization of Biomaterials Using Simulated Body Fluids (SBFs) for Bone Tissue Engineering and Regenerative Medicine. *Tissue Engineering Part A* **0**:ja. . [Abstract] [Full Text PDF] [Full Text PDF with Links]
4. Eiji Saito, Darilis Suarez-Gonzalez, William L. Murphy, Scott J. Hollister. 2015. Biomineral Coating Increases Bone Formation by Ex Vivo BMP-7 Gene Therapy in Rapid Prototyped Poly(l -lactic acid) (PLLA) and Poly(ε-caprolactone) (PCL) Porous Scaffolds. *Advanced Healthcare Materials* **4**:4, 621-632. [Crossref]
5. Scott J. Hollister, Colleen L. Flanagan, David A. Zopf, Robert J. Morrison, Hassan Nasser, Janki J. Patel, Edward Ebramzadeh, Sophia N. Sangiorgio, Matthew B. Wheeler, Glenn E. Green. 2015. Design Control for Clinical Translation of 3D Printed Modular Scaffolds. *Annals of Biomedical Engineering* **43**:3, 774-786. [Crossref]
6. Qingqiang Yao, Bo Wei, Yang Guo, Chengzhe Jin, Xiaotao Du, Chao Yan, Junwei Yan, Wenhao Hu, Yan Xu, Zhi Zhou, Yijin Wang, Liming Wang. 2015. Design, construction and mechanical testing of digital 3D anatomical data-based PCL–HA bone tissue engineering scaffold. *Journal of Materials Science: Materials in Medicine* **26**:1. . [Crossref]
7. Joel D Boerckel, Devon E Mason, Anna M McDermott, Eben Alsberg. 2014. Microcomputed tomography: approaches and applications in bioengineering. *Stem Cell Research & Therapy* **5**:6, 144. [Crossref]
8. Doo Yeon Kwon, Jin Seon Kwon, Sun Woo Shim, Ji Hoon Park, Junhee Lee, Jae Ho Kim, Wan-Doo Kim, Moon Suk Kim. 2014. Preparation of three-dimensional scaffolds by using solid freeform fabrication and feasibility study of the scaffolds. *Journal of Materials Chemistry B* **2**:12, 1689. [Crossref]
9. Min Jae Song, David Dean, Melissa L. Knothe Tate. 2013. Mechanical modulation of nascent stem cell lineage commitment in tissue engineering scaffolds. *Biomaterials* **34**:23, 5766-5775. [Crossref]